CODEE Journal

Volume 12 *Linking Differential Equations to Social Justice and Environmental Concerns*

Article 3

2-13-2019

The Ocean and Climate Change: Stommel's Conceptual Model

James Walsh
Oberlin College

The Ocean and Climate Change: Stommel's Conceptual Model

James A. Walsh
Oberlin College

Keywords: Overturning circulation, density gradients, stable nodes, bifurcation
Manuscript received on December 19, 2018; published on February 13, 2019.

Abstract: The ocean plays a major role in our climate system and in climate change. In this article we present a conceptual model of the Atlantic Meridional Overturning Circulation (AMOC), an important component of the ocean's global energy transport circulation that has, in recent times, been weakening anomalously. Introduced by Henry Stommel, the model results in a two-dimensional system of first order ODEs, which we explore via *Mathematica*. The model exhibits two stable regimes, one having an orientation aligned with today's AMOC, and the other corresponding to a reversal of the AMOC. This material is appropriate for a junior-level mathematical modeling or applied dynamical systems course.

1 Introduction

That our climate is changing is difficult to dispute. The most recent assessment report of the Intergovernmental Panel on Climate Change (IPCC AR5) concludes [8]:

> Warming of the climate system is unequivocal, and since the 1950s, many of the observed changes are unprecedented over decades to millennia. The atmosphere and ocean have warmed, the amounts of snow and ice have diminished, sea level has risen, and the concentrations of greenhouse gases have increased.

IPCC AR5 also provides strong evidence indicating that human activities, such as the burning of fossil fuels, have contributed significantly to this warming trend.

The ocean plays a major role in our climate system. For example, the ocean has a remarkable capacity for absorbing large amounts of atmospheric CO_2, a potent greenhouse gas. It is estimated that the ocean has absorbed 40% of all anthropogenic CO_2 emissions since the beginning of the industrial era, with the rate of uptake by the ocean increasing in the 2000s [3].

The focus in this article, however, will be placed on a second crucial aspect of the ocean's role in shaping our climate, namely, its capacity for transporting vast amounts of energy. The Thermohaline Circulation (THC) is the major global ocean circulation

pattern, with the rate of flow determined by density contrasts which, in turn, are functions of temperature and salinity (*thermo*–heat; *haline*–salt).

The Atlantic Meridional Overturning Circulation (AMOC), one component of the THC, consists of the northward flow of warm, upper-ocean waters to the North Atlantic, and the deep southward return flow of denser water that forms through the process of cooling and sinking at high latitudes (this latter phenomenon is known as *deep water formation*). Changes in the strength of the AMOC alter this important process of heat transport to northern latitudes, with cooling in the subtropical North Atlantic and colder climates along coastal areas of Europe being potential consequences.

The AMOC has indeed weakened over the past 150 years, a change that is anomalous relative to the preceding 1500 years [10]. Thornalley et al suggest that enhanced freshwater fluxes from melting glaciers into the North Atlantic in the middle of the 19th century—at the end of a cool period known as the Little Ice Age—resulted in less dense water and reduced deep water formation, weakening the AMOC. Currently, with ongoing reductions in the mass of the Greenland ice sheet (along with other factors), scientists believe further slowing of the AMOC is very likely in the coming decades [7]. As it stands, the current weakening of the AMOC is playing an essential role in distressing several marine species in the Gulf of Maine [2].

Changes in the strength of the AMOC have a profound effect on climate. Going back further in time, the last ice age saw repeated, millennial climate oscillations—relatively colder and warmer periods within the ice age itself—the most pronounced occurring between twenty-five and sixty thousand years ago. Analysis of data from ocean sediment cores shows the AMOC weakened during every colder phase, while relatively warmer periods followed a reinvigoration of the overturning circulation [4]. This work of L.G. Henry et al provides direct evidence of the central role played by the ocean, and the AMOC in particular, in significant climate change.

The AMOC is driven by density contrasts, with water density a decreasing function of temperature and an increasing function of salinity. In his pioneering 1961 paper [9], Henry Stommel introduced a conceptual 2-reservoir ocean box model to investigate the density-driven flow between the boxes. The water flows through a connecting, bottom capillary, with a compensating overflow at the top (in sum representing the "overturning circulation"). Interestingly, Stommel found coexisting stable regimes, one for each direction of flow through the capillary. The fact these two distinct stable regimes can occur in such an idealized model lead Stommel to wonder if a similar situation might occur in nature. If the AMOC, for example, possessed a stable motion having a direction of flow the reverse of that which we have today, might a sufficient perturbation of our climate system cause the AMOC to jump to this other regime?

Stommel's model results in a pair of first order ODEs and, as such, its study is appropriate for a modeling course or a class focusing on the qualitative and/or numerical investigation of planar systems of ODEs. (I present Stommel's model in a climate modeling course having the sophomore-level ODE course as a prerequisite.) While providing no real predictive power, Stommel's conceptual model does allow for investigations into the manner in which fundamental factors such as water temperature and salinity influence density contrasts, and thus the strength and direction of an idealized flow between two basins.

Motivating 1-box models are introduced in Sections 2 and 3 to investigate the interactions between temperature, salinity, and flow rate as they influence the density of a water parcel over time. In particular, these simple models help set the stage for Stommel's more sophisticated 2-box model, presented in Section 4. As mentioned above, there is a feedback in the sense that flow rate in turn affects the density. To introduce this feedback, a second reservoir is added to the model and the corresponding 2-dimensional system of ODEs is derived in Section 4. The dynamics of the model are investigated, with the aid of *Mathematica*, in Section 5. We discuss bifurcations and the associated hysteresis exhibited by the model in Section 5 as well. Concluding remarks are presented in the final section.

2 A 1-Basin Model

Consider a well-mixed reservoir of water with uniform temperature $T = T(t)$ (°C) and uniform salinity $S = S(t)$. The quantity S is defined as a concentration and is measured in practical salinity units (psu), a dimensionless unit. Porous walls separate the basin from an outer vessel having constant temperature T^* and constant salinity S^* (Figure 1). The outer vessel might, for example, represent a neighboring ocean.

Assume the transfer of heat and salt between the reservoir and outer vessel is modeled simply by

$$\begin{aligned} \frac{dT}{dt} &= c(T^* - T) \\ \frac{dS}{dt} &= d(S^* - S), \end{aligned} \tag{2.1}$$

where $c > 0$ and $d > 0$ are constants. Students can be asked to show the general solution of (2.1) is

$$(T(t), S(t)) = (T^* + (T_0 - T^*)e^{-ct},\ S^* + (S_0 - S^*)e^{-dt}), \quad (T_0, S_0) = (T(0), S(0)).$$

Every solution of (2.1) converges to the equilibrium (T^*, S^*) as $t \to \infty$ in this setting.

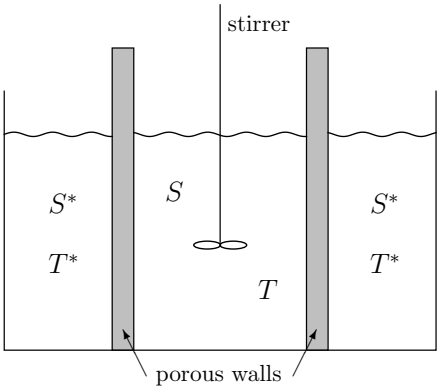

Figure 1: The outer vessel has constant salinity S^* and temperature T^*. Heat and salinity are exchanged with the outer vessel through porous walls.

2.1 Nondimensionalization

Note system (2.1) contains the four parameters c, d, T^* and S^*. The number of parameters can be reduced by *nondimensionalizing*; letting $x = S/S^*$, we have

$$\frac{dx}{dt} = \frac{1}{S^*}\frac{dS}{dt} = \frac{1}{S^*}(d(S^* - S)) = d(1 - x).$$

Similarly, setting $y = T/T^*$ yields

$$\frac{dy}{dt} = \frac{1}{T^*}\frac{dT}{dt} = \frac{1}{T^*}(c(T^* - T)) = c(1 - y).$$

Note variables x and y are dimensionless; additionally, we now only have two parameters.

A further simplification can be realized by rescaling time; setting $\tau = ct$ yields

$$\frac{dx}{d\tau} = \frac{dx}{dt}\frac{dt}{d\tau} = \frac{1}{c}(d(1 - x)) = \delta(1 - x) \quad \text{and} \quad \frac{dy}{d\tau} = \frac{dy}{dt}\frac{dt}{d\tau} = \frac{1}{c}(c(1 - y)) = (1 - y),$$

where $\delta = d/c$ is the (dimensionless) ratio of the rates at which salinity and temperature approach equilibrium. Letting "$'$" denote $\frac{d}{d\tau}$, we have

$$\begin{aligned} x' &= \delta(1 - x) \\ y' &= 1 - y, \end{aligned} \tag{2.2}$$

a system with the single parameter δ. Given that thermal energy generally transfers on a faster time scale than does salinity, Stommel chooses $\delta = 1/6$, so that temperature equilibrates much more quickly than does salinity (Figure 2).

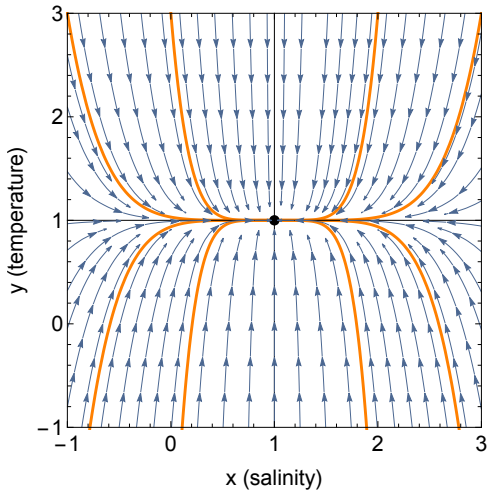

Figure 2: Phase plane for system (2.2) with $\delta = 1/6$. All solutions tend to $(1, 1)$, with y (temperature) equilibrating more quickly than x (salinity).

2.2 Density Anomaly

Recall that temperature and salinity work in an opposing fashion in determining density. One might ask what happens to the density over time if, for example, salinity and temperature each increase toward equilibrium. Let Γ denote the solution to system (2.2) with initial condition $(x(0), y(0)) = (0, 0)$ (so that $x(t)$ and $y(t)$ each increase toward 1 as $t \to \infty$). Given that density is an increasing function of salinity and a decreasing function of temperature, a simple approach is to let

$$\rho = \rho_0(1 - \alpha T + \beta S), \tag{2.3}$$

where ρ (gm/cm^3) is the density, ρ_0 is a reference density (here corresponding to the density at $T = S = 0$), and α ($^\circ$C^{-1}) and β (psu^{-1}) are positive constants. Using $T = yT^*$ and $S = xS^*$, we have

$$\rho = \rho_0(1 - \alpha y T^* + \beta x S^*) = \rho_0(1 + \alpha T^*(-y + Rx)), \tag{2.4}$$

where $R = \beta S^*/\alpha T^*$ is a positive, dimensionless constant measuring the relative effect of salinity and temperature on density.

At the equilibrium point $(x, y) = (1, 1)$, $\rho' = \rho_0(1 + \alpha T^*(-1 + R))$. The density at equilibrium will thus be greater than at $(x, y) = (0, 0)$ if $R > 1$; following Stommel, we set $R = 2$.

One might then ask if the density increases monotonically along Γ as x and y approach equilibrium. Using (2.4) and equations (2.2), note

$$\rho' = \rho_0 \alpha T^*(-y' + Rx') = \rho_0 \alpha T^*(-1 + y + R\delta(1 - x)).$$

When $x = y = 0$, $\rho' = \rho_0 \alpha T^*(-1 + R\delta) < 0$ since $R = 2$ and $\delta = 1/6$. Thus, starting at $(x, y) = (0, 0)$, the density first decreases, due to the larger time constant for temperature, as T rapidly approaches equilibrium. Given sufficient time, however, salinity becomes the dominant factor as it increases toward equilibrium (via long-term evaporation, say), resulting in an eventual increase in density.

The interplay between temperature and salinity vis-à-vis density described above can be viewed in the (dimensionless) *density anomaly*

$$\sigma = \frac{1}{\alpha T^*}\left(\frac{\rho}{\rho_0} - 1\right) = -y + Rx, \tag{2.5}$$

which follows from (2.4). The term anomaly is used as σ is proportional to $\rho - \rho_0$ so that, starting at $x = y = 0$, whether the water becomes more or less dense over time is indicated by whether $\rho - \rho_0 > 0$ or $\rho - \rho_0 < 0$. Level sets of σ, along with the trajectory Γ, are plotted in Figure 3. Note the density anomaly $\sigma < 0$ on $(0, \hat{t})$ due to the influence of increasing temperature, and $\sigma > 0$ on $(\hat{t}, \infty)$ as salinity continues to increase ($\hat{t}$ as in Figure 3).

While model (2.1) has been introduced to investigate the dynamics of the density as temperature and salinity evolve in the simplest of settings, the following section presents an augmented model incorporating flow rate and the effect flow rate has on density.

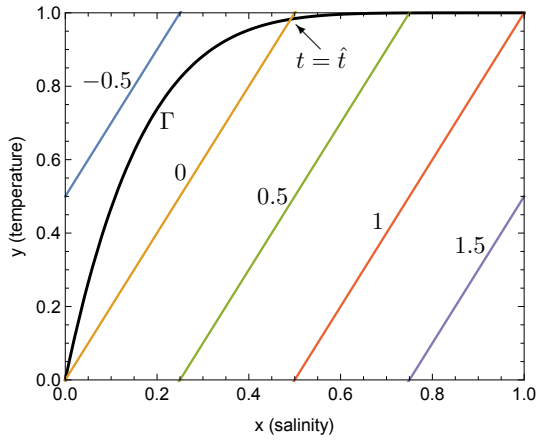

Figure 3: Level sets of the density anomaly σ (2.5) (colored lines) and the trajectory of the solution Γ starting at $(x, y) = (0, 0)$. The water in the basin is less dense than at $(x, y) = (0, 0)$ for $t \in (0, \hat{t})$, and more dense for $t > \hat{t}$.

3 A 1-Basin Model with Inflow and Outflow

To consider the effects flow rate may have on density, imagine an external inflow of water having fixed temperature $T = T_{in}$ and fixed salinity $S = S_{in}$ at a rate q (s^{-1}). Basin water having temperature T and salinity S exits the reservoir at the same rate q (see Figure 4). The equation for the temperature of the basin water is now

$$\frac{dT}{dt} = c(T^* - T) + q\,T_{in} - q\,T.$$

To simplify matters, shift the origin of the temperature axis to T_{in} by setting $u = T - T_{in}$. Note

$$\begin{aligned}\frac{du}{dt} = \frac{dT}{dt} &= c(T^* - u - T_{in}) + q\,T_{in} - q(u + T_{in}) \\ &= c(u^* - u) - qu,\end{aligned}$$

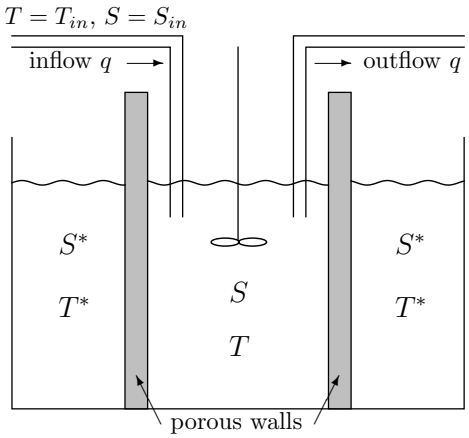

Figure 4: The 1-box, inflow/outflow model. The incoming water has fixed temperature $T = T_{in}$ and fixed salinity $S = S_{in}$.

where $u^* = T^* - T_{in}$. Similarly, after setting $v = S - S_{in}$ and letting $v^* = S^* - S_{in}$, the salinity equation becomes

$$\frac{dv}{dt} = d(v^* - v) - qv.$$

Note that in the (u, v)-coordinate system it is the evolution of temperature and salinity relative to T_{in} and S_{in}, respectively, that is being modeled.

As above, we nondimensionalize by letting $x = v/v^*$, $y = u/u^*$ and $\tau = ct$ to reduce the number of parameters. One can easily check these substitutions result in the system

$$\begin{aligned} x' &= \delta - (\delta + f)x \\ y' &= 1 - (1 + f)y, \end{aligned} \tag{3.1}$$

where $\delta = d/c$ as before, and $f = q/c$ is a (new) dimensionless flow rate.

Note the equilibrium solution of (3.1) has the form

$$(x^*, y^*) = \left(\frac{\delta}{\delta + f}, \frac{1}{1 + f}\right). \tag{3.2}$$

Let ρ_0 denote the density of the basin water when $(u, v) = (0, 0)$, that is, when $(T, S) = (T_{in}, S_{in})$. Setting $\rho = \rho_0(1 - \alpha u + \beta v)$ and proceeding as in the previous section, the density anomaly at equilibrium becomes

$$\sigma^* = \frac{1}{\alpha u^*}\left(\frac{\rho}{\rho_0} - 1\right) = -y^* + Rx^* = -\frac{1}{1 + f} + \frac{R\delta}{\delta + f}. \tag{3.3}$$

Note that we have made use of (3.2).

If we set $f = 0$ in (3.2) and (3.3) (so $q = 0$ and the inflow and outflow are turned off), we recover $(x^*, y^*) = (1, 1)$ and $\sigma^* = -1 + R = 1 > 0$, as in Section 2. As the flow rate $f \to \infty$, however, $(x^*, y^*) \to (0, 0)$ and $\sigma^* \to 0$. We thus see that the density anomaly at equilibrium varies with the flow rate. Indeed, plotting the density anomaly at equilibrium σ^* as a function of the flow rate f (Figure 5), we see the outflow is more dense than the inflow water if $f \in (0, 1/4)$, while the outflow is less dense than the inflow water if $f \in (1/4, \infty)$.

This simple model illustrates the role flow rate plays in determining water density in the basin. For a very slow inflow/outflow, an incoming parcel of water resides in the basin for an extended time, during which the salinity comes to dominate the density as discussed in Section 2. For fast inflow/outflow rates, temperature has the dominating short-term effect and the outflow water is then less dense than the inflow.

The AMOC is driven by density contrasts, as mentioned above. In this section we have seen the flow rate influences density, so that there is a feedback between flow rate and density. To investigate this feedback a second basin will be added to the model, as described in the following section.

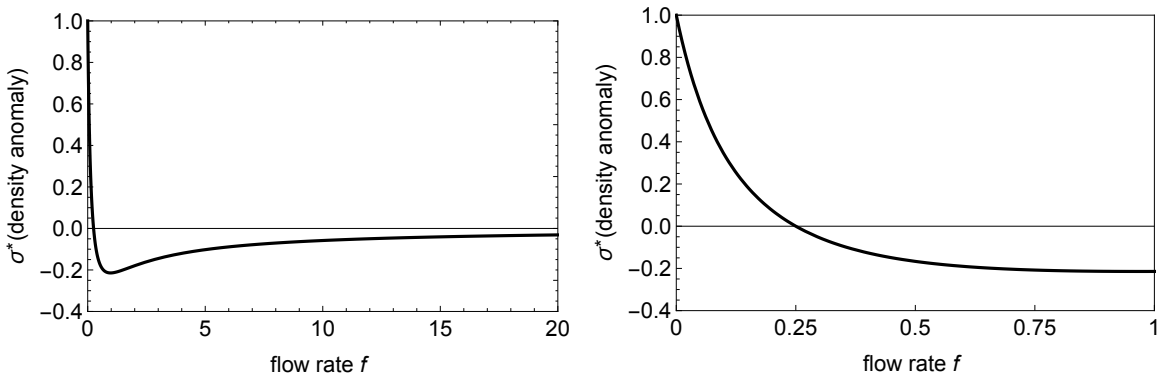

Figure 5: The density anomaly at equilibrium as a function of flow rate f. *Left*: $0 < f < 20$. *Right*: $0 < f < 1$. Small flow rates lead to outflow more dense than the inflow; larger flow rates lead to outflow less dense than the inflow.

4 Stommel's 2-Box Model

4.1 Model Equations

Consider two well-mixed basins of water connected at the bottom by a capillary, with a corresponding overflow at the top so as to maintain constant volume in each basin. There is an exchange of heat and salinity with outer vessels having constant temperature T_i^* and salinity $S_i^*,\ i = 1, 2$ (see Figure 6).

Let $T_i(t)$ and $S_i(t)$ denote the temperature and salinity of the water in box $i,\ i = 1, 2$. The direction and strength of the flow through the capillary is driven by the difference in densities of the two boxes. If $S_1 = S_2$, for example, the colder box will contain denser water and the flow will be from the colder to the warmer box. This would then correspond to a flow of water from the cooler high latitudes to the warmer low latitudes (as is currently the case with deep water formation and the AMOC).

If $T_1 = T_2$, however, then salinity will determine the difference in densities. Due to

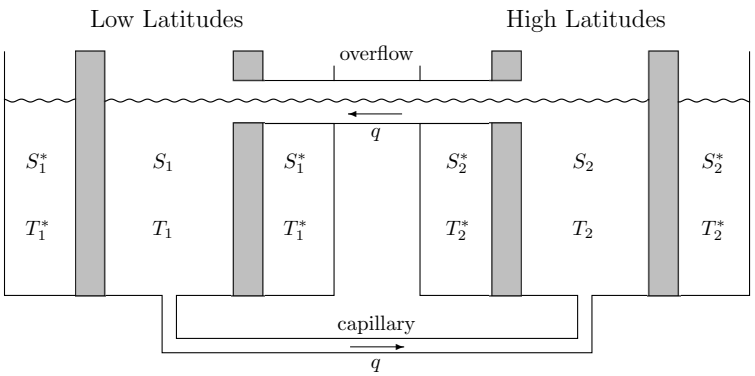

Figure 6: Stommel's 2-box model. The direction of flow through the capillary is driven by density differences. As pictured here, the capillary (deep water) flow is from the low latitude (warm) box to the high latitude (cold) box.

increased evaporation in lower latitudes, with a resulting increase in salinity of the ocean water, the lower latitude box will be the saltier of the two. Hence if $T_1 = T_2$, the saltier box will contain denser water and the flow will be from the warmer to the colder box. This would then correspond to a flow of water from the warmer low latitudes to the cooler high latitudes.

We note that water in the high latitude box is colder but less salty, while the water in the low latitude box is warmer but saltier, so the direction of the flow is, generally, not clear.

Let's first derive the temperature equations for the 2-box model. Referring to Figure 6, the equations are

$$\begin{aligned} \frac{dT_1}{dt} &= c(T_1^* - T_1) + q\,T_2 - q\,T_1 \\ \frac{dT_2}{dt} &= c(T_2^* - T_2) - q\,T_2 + q\,T_1. \end{aligned} \tag{4.1}$$

Note equations (4.1) remain unchanged if the direction of the flow is reversed, due to the compensating overflow at the top of the basins. We thus have

$$\frac{dT_1}{dt} = c(T_1^* - T_1) + |q|(T_2 - T_1) \tag{4.2a}$$

$$\frac{dT_2}{dt} = c(T_2^* - T_2) - |q|(T_2 - T_1). \tag{4.2b}$$

It is once again convenient to shift the temperature axes, here setting $u_i = T_i - T^*_{ave}$, $i = 1, 2$, where $T^*_{ave} = \frac{1}{2}(T_1^* + T_2^*)$. Equation (4.2a) becomes

$$\begin{aligned} \frac{du_1}{dt} = \frac{dT_1}{dt} &= c(T_1^* - u_1 - T^*_{ave}) + |q|(u_2 + T^*_{ave} - u_1 - T^*_{ave}) \\ &= c(T_1^* - T^*_{ave} - u_1) + |q|(u_2 - u_1), \end{aligned}$$

while (4.2b) becomes

$$\begin{aligned} \frac{du_2}{dt} = \frac{dT_2}{dt} &= c(T_2^* - u_2 - T^*_{ave}) - |q|(u_2 + T^*_{ave} - u_1 - T^*_{ave}) \\ &= c(T_2^* - T^*_{ave} - u_2) - |q|(u_2 - u_1). \end{aligned}$$

Let $u^* = T_1^* - T^*_{ave}$, and note $T_2^* - T^*_{ave} = -u^*$. Hence in (u_1, u_2)-coordinates the temperature equations become

$$\frac{du_1}{dt} = c(u^* - u_1) + |q|(u_2 - u_1) \tag{4.3a}$$

$$\frac{du_2}{dt} = c(-u^* - u_2) - |q|(u_2 - u_1). \tag{4.3b}$$

The net effect of the (u_1, u_2)-change of variables is that one may assume the temperatures in the outer vessels are the opposite of each other.

In an entirely analogous manner, the salinity equations are

$$\frac{dS_1}{dt} = d(S_1^* - S_1) + |q|(S_2 - S_1) \tag{4.4a}$$

$$\frac{dS_2}{dt} = d(S_2^* - S_2) - |q|(S_2 - S_1). \tag{4.4b}$$

If we let $v_i = S_i - S_{ave}^*$, $i = 1, 2$, where $S_{ave}^* = \frac{1}{2}(S_1^* + S_2^*)$, and $v^* = S_1^* - S_{ave}^*$, the salinity equations in the (v_1, v_2)-coordinate system become

$$\frac{dv_1}{dt} = d(v^* - v_1) + |q|(v_2 - v_1) \tag{4.5a}$$

$$\frac{dv_2}{dt} = d(-v^* - v_2) - |q|(v_2 - v_1). \tag{4.5b}$$

Note that addition of the equations in system (4.3) yields $\frac{d}{dt}(u_1 + u_2) = -c(u_1 + u_2)$. We see that for any initial condition, $(u_1 + u_2)(t) \to 0$ as $t \to \infty$. We will thus simplify matters by assuming $u_1 = -u_2 = u$ in all that follows.

In a similar fashion, addition of the equations in system (4.5) yields $\frac{d}{dt}(v_1 + v_2) = -d(v_1 + v_2)$. Hence, given that $(v_1 + v_2)(t) \to 0$ as $t \to \infty$ for any initial condition, we assume $v_1 = -v_2 = v$ henceforth. Making these substitutions into (4.3a) and (4.5a) results in the two dimensional system of equations

$$\begin{aligned} \frac{du}{dt} &= c(u^* - u) - 2|q|u \\ \frac{dv}{dt} &= d(v^* - v) - 2|q|v. \end{aligned} \tag{4.6}$$

Solving system (4.6) will yield the temperature and salinity of the water in basin one as a function of time, with each of the temperature and salinity of the water in basin two then the opposite of that in basin one.

As in previous sections, nondimensionalizing proves helpful. Letting $x = v/v^*$, $y = u/u^*$ and $\tau = ct$, the reader is invited to show that system (4.6) becomes

$$\begin{aligned} x' &= \delta(1 - x) - |f|x \\ y' &= 1 - y - |f|y, \end{aligned} \tag{4.7}$$

where "$'$" denotes $\frac{d}{d\tau}$, $\delta = d/c$, and $f = 2q/c$ is a nondimensionalized flow rate.

4.2 Density Driven Flow

The reader may note (4.7) and the 1-basin model (3.1) each contain a "flow" parameter. The advantage of incorporating a second basin is that f in (4.7) can now be made to depend upon density, which in turn is a function of x and y. Following Stommel, assume the flow rate is proportional to the difference in densities in the two boxes, that is, $kq = \rho_1 - \rho_2$, where k (s gm/cm^3) is a positive constant (we take the capillary flow orientation depicted

in Figure 6 to represent $q > 0$). Recalling relation (2.3) and our symmetry assumption $u_2 = -u_1$ and $v_2 = -v_1$, we have

$$\begin{aligned} kq &= \rho_0(1 - \alpha u_1 + \beta v_1) - \rho_0(1 - \alpha u_2 + \beta v_2) \\ &= \rho_0(-\alpha(u_1 - u_2) + \beta(v_1 - v_2)) \\ &= 2\rho_0(-\alpha u + \beta v) \\ &= 2\rho_0 \alpha u^*(-y + Rx), \end{aligned} \tag{4.8}$$

where we have used $x = v/v^*$, $y = u/u^*$ and $R = \beta v^*/\alpha u^*$.

Notably, we see the flow rate q is a function of salinity x and temperature y. If $y > Rx$, so that temperature dominates the density difference, $q < 0$ and the deep water flow is the reverse of that pictured in Figure 6, from the cold box to the warm box. In this case water flows from the colder high latitudes to the warmer low latitudes. For $Rx > y$, however, salinity plays the leading role and the capillary flow is as in Figure 6 ($q > 0$), now from the saltier to the less salty box. In this scenario water moves from the warmer low latitudes to the colder high latitudes, the reverse of the current orientation of the AMOC.

The dependence of the flow rate f on salinity x and temperature y in system (4.7) can be made explicit. To that end, since $f = 2q/c$ we have $kq = kcf/2$, from which it follows via (4.8) that

$$-y + Rx = \lambda f, \quad \text{where} \quad \lambda = \frac{kc}{4\rho_0 \alpha u^*}. \tag{4.9}$$

System (4.7) becomes

$$\begin{aligned} x' &= \delta(1 - x) - \tfrac{1}{\lambda}|y - Rx|\, x \\ y' &= 1 - y - \tfrac{1}{\lambda}|y - Rx|\, y. \end{aligned} \tag{4.10}$$

We note that, while not continuously differentiable, the vector field defined by (4.10) is Lipschitz continuous so (4.10) admits a unique solution for any initial condition $(x(0), y(0))$.

While a qualitative approach to the analysis of the nonlinear system (4.10) is feasible in an upper-level course (see [5], Chapter 6), here we make use of the *Mathematica* notebook in the Appendix to determine model behavior.

5 Dynamics of the 2-Box Model

With a bit of algebra, one can show solving system (4.10) for equilibrium solutions reduces to the finding of roots of a cubic polynomial in x; hence (4.10) will typically have one or three real equilibrium solutions (x^*, y^*). Looking to keep the flow rate involved, note that at equilibrium

$$\begin{aligned} x' &= \delta(1 - x) - |f|x = 0 \\ y' &= 1 - y - |f|y = 0, \end{aligned}$$

from which it follows an equilibrium point satisfies

$$x^* = \frac{\delta}{\delta + |f|} \quad \text{and} \quad y^* = \frac{1}{1 + |f|}. \tag{5.1}$$

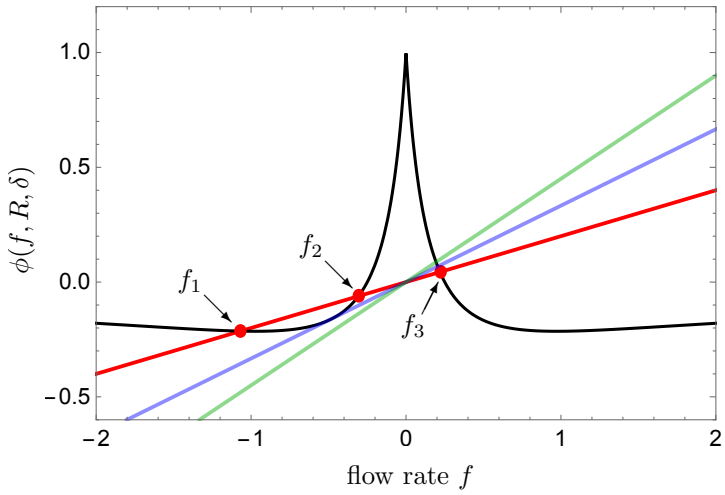

Figure 7: *Black*: Plot of $\phi(f, R, \delta)$ with $R = 2$, $\delta = 1/6$. Lines are plots of λf with $\lambda = 1/5$ (*red*), $\lambda = 1/3$ (*blue*) and $\lambda = 2/5$ (*green*). The f_i are equilibrium flow rates, $i = 1, 2, 3$.

From equation (4.9),

$$\lambda f = -y^* + Rx^* = -\frac{1}{1 + |f|} + \frac{R\delta}{\delta + |f|} \equiv \phi(f, R, \delta). \tag{5.2}$$

Solutions of equation (5.2) for the flow rate f can then be substituted into (5.1) to determine the equilibrium point(s) (x^*, y^*).

The black curve in Figure 7 is the graph of $\phi(f, 2, 1/6)$, while the red line in Figure 7 is the graph of λf for $\lambda = 1/5$; the intersection of these two curves will yield f-values satisfying (5.2). We see for the given parameters equation (5.2) has three real solutions, which we label $f_1 < f_2 < f_3$, while the corresponding equilibrium solutions of system (4.10) will be denoted (x_i^*, y_i^*), $i = 1, 2, 3$.

Given that $f_i < 0, i = 1, 2$, temperature dominates density differences and the flow through the capillary is from the cold box to the warm box when the system is in equilibrium states (x_i^*, y_i^*), $i = 1, 2$. At equilibrium (x_3, y_3), however, $f_3 > 0$ and salinity dominates density differences; the capillary flow is now from the warm box to the cold box as in Figure 6.

We use *Mathematica* to investigate the stability of each equilibrium solution via the file appended to this article. Presented in Table 1 are the eigenvalues of the Jacobian matrices $J(x_i^*, y_i^*)$ when $\lambda = 1/5, R = 2$ and $\delta = 1/6$ (we fix $R = 2$ and $\delta = 1/6$ in all that follows). For $\lambda = 1/5$, we see (x_1^*, y_1^*) is a stable node and (x_3^*, y_3^*) is a stable spiral, while (x_2^*, y_2^*) is a saddle. This conceptual model exhibits two stable regimes, one in which temperature drives the density difference and the deep water flow is from the cold box to the warm box, the other having salinity dominate the density difference with the capillary flow going from the warm box to the cold box. As mentioned above, this result caused Stommel to wonder whether such a situation might occur in nature.

To further investigate the dynamics of (4.10), we plot the xy-phase plane in Figure 8. The green line in Figure 8 corresponds to $f = 0$; above this line the flow is from the cold box to the warm box, with temperature dominating, and below the flow is from the

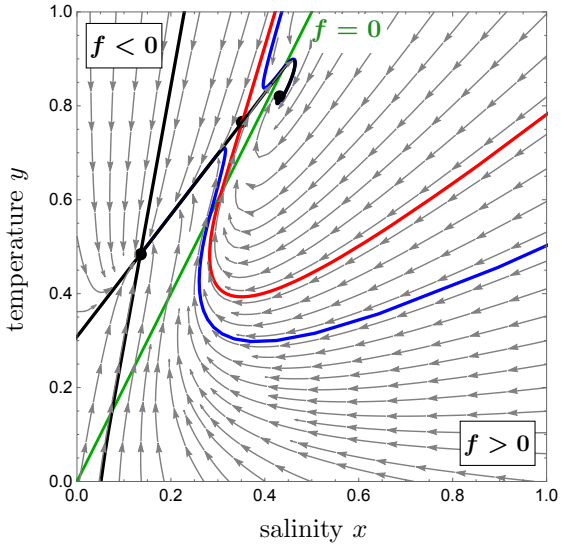

Figure 8: The xy-phase plane for $\lambda = 1/5, R = 2, \delta = 1/6$. The black dots are equilibria (x_i^*, y_i^*), with $x_1 < x_2 < x_3$. The red curve is the stable separatrix for the saddle point. The flow through the capillary reverses direction on each of the blue trajectories.

warm box to the cold box with salinity dominating. Note in particular the existence of trajectories that cross the $f = 0$ line (the blue curves in Figure 8 are two such trajectories). Hence there are initial conditions for which the deep water flow slows down and then reverses over time.

f equilibrium values	(x^*, y^*) equilibrium values	Jacobian $J(x^*, y^*)$ eigenvalues	equilibrium type
$f_1 = -1.068$	$(x_1^*, y_1^*) = (0.135, 0.484)$	$-3.609,\ -0.761$	stable node
$f_2 = -0.307$	$(x_2^*, y_2^*) = (0.352, 0.765)$	$-2.849,\ 0.761$	saddle
$f_3 = 0.219$	$(x_3^*, y_3^*) = (0.432, 0.820)$	$-0.921 \pm 1.823\, i$	stable spiral

Table 1. Parameters $\lambda = 1/5,\ R = 2,\ \delta = 1/6$.

5.1 Bifurcations and Hysteresis

In this section we briefly discuss bifurcations and associated hysteresis exhibited by the model. To set the stage, denote by $\mathcal{B}_i$ the set of initial conditions for which the corresponding solution of (4.10) converges to (x_i^*, y_i^*) as $t \to \infty, i = 1, 2, 3$ (the sets $\mathcal{B}_i$ are called *basins of attraction*). Note the stable separatrix of the saddle (the red curve in Figure 8) separates $\mathcal{B}_1$ and $\mathcal{B}_3$, the basins of attraction of the two stable equilibria. For the parameter values used in Figure 8, the system would require a large perturbation to enable a solution near the stable node (x_1^*, y_1^*) to jump over to $\mathcal{B}_3$ (and so cause a reversal of the deep water flow).

What happens if we vary the parameter λ, a proportionality constant for the flow rate f via (4.9)? An increase in λ, which may correspond to factors such as increased bottom friction or greater wind-driven surface turbulence [5], makes it more difficult for the water to flow from one basin to the other. A decrease in λ, on the other hand, would make it easier for water to flow through the capillary.

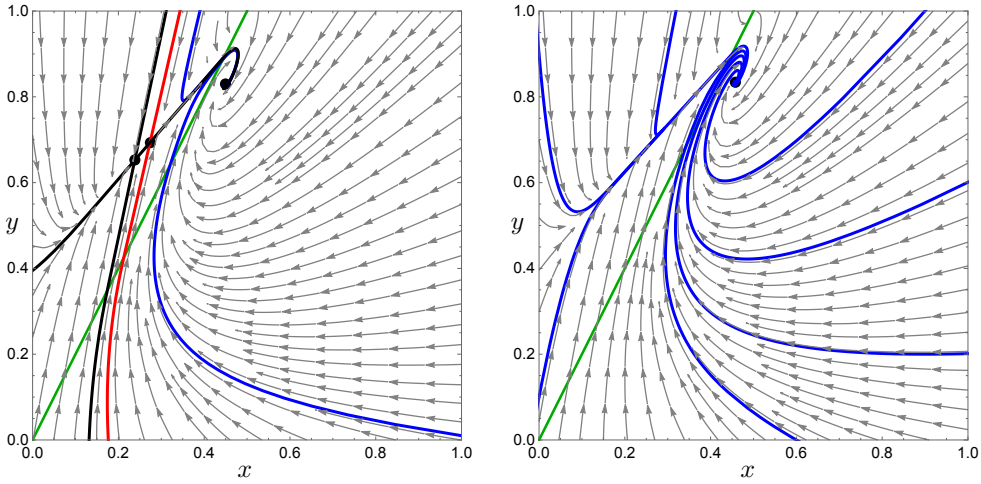

Figure 9: The xy-phase planes for $\lambda = 1/3$ (left) and $\lambda = 2/5$ (right).

The blue line in Figure 7 is the plot of λf for $\lambda = 1/3$. While difficult to discern in this image, there are again three equilibrium flow rates $f_1 < f_2 < 0 < f_3$ (f_1 and f_2 are quite close together). The stability type of equilibria (x_i^*, y_i^*), $i = 1, 2, 3$, remains unchanged from the $\lambda = 1/5$ case, as can be investigated via the *Mathematica* file in the Appendix.

The left plot in Figure 9 is the xy-phase plane for $\lambda = 1/3$. Note the stable node (x_1^*, y_1^*) and the saddle (x_2^*, y_2^*) are close to merging. Here, a solution near (x_1^*, y_1^*) within $\mathcal{B}_1$ would need but a slight nudge to jump to $\mathcal{B}_3$, with a corresponding reversal of the flow.

The green line in Figure 7 is the graph of λf for $\lambda = 2/5$. There is now but one equilibrium flow rate $f_1 > 0$. The stable node (x_1^*, y_1^*) and the saddle (x_2^*, y_2^*) merge at some $\lambda_0 \in (1/3, 2/5)$, disappearing as λ increases through λ_0 via a *saddle-node bifurcation* ([1], §9.3). For $\lambda = 2/5$ the system is permanently stuck in the regime in which the deep water flow is from the warm box to the cold box, with salinity dominating the density difference (right plot in Figure 9).

The *bifurcation plot* in Figure 10, in which the equilibrium flow rate is plotted as a function of the flow resistance λ, summarizes the above discussion. The red and green portions of the curve correspond to stable equilibria for system (4.10) (stable node and stable spiral, respectively), while the blue portion corresponds to the unstable saddle point. As λ increases through λ_0, the flow rate jumps to the green curve; such a bifurcation is often referred to as a *tipping point* by climate scientists.

Interestingly, the model also exhibits the following behavior. If we start on the stable red curve in Figure 10 at $\lambda = 1/5$, and first increase λ through λ_0 so that f jumps to the green stable curve, and then decrease λ back to $\lambda = 1/5$, f remains on the stable green curve. That is, the system is in a different stable regime than the one in which it started, even though the parameter values are the same. This phenomenon, known as *hysteresis*, is presented in [10] as a possible explanation for evidence suggesting that the AMOC has yet to recover from the weakening of the flow that began at the end of the Little Ice Age.

The appearance of hysteresis in Stommel's model is perhaps suggestive of the possibility that, were the AMOC to slow down and switch orientation due to climate change, any future return to the current transport of warm surface waters to the North Atlantic will be difficult to realize.

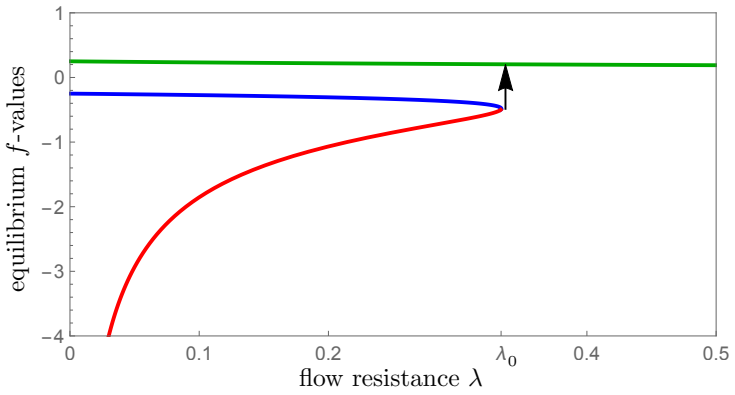

Figure 10: f-equilibrium values as a function of λ. *Red*: stable node (x_1^*, y_1^*). *Blue*: saddle (x_2^*, y_2^*). *Green*: stable spiral (x_3^*, y_3^*). System (4.10) has a saddle-node bifurcation at $\lambda = \lambda_0$.

6 Discussion

Stommel's 2-box model is conceptual in nature, a greatly simplified model of but one component of the global ocean circulation. No consideration is given to the coupling of the subpolar North Atlantic ocean with other oceans or with the atmosphere. Nevertheless, that such a simple model exhibits stable regimes having oppositely oriented circulation patterns, and that the passing from one circulation mode to the other can be induced by changing forcing parameters, has had a significant impact on climate science and oceanography [5].

L.G. Henry et al found that repeated weakening of the AMOC on a millenial time scale during cycles of temperature fluctuations in the last ice age occurred during each of the relatively colder periods, the latter coinciding with immense discharges of freshwater from melting ice in Canada into the subpolar North Atlantic [4]. Similarly, the work of Thornally et al suggests that increased freshwater fluxes from melting glaciers and sea ice roughly 150 years ago served to weaken the AMOC, anomalously so with respect to the past 1,500 years [10].

The effect of these "freshwater forcings" can be seen in Stommel's model: assuming the capillary flow is from the colder to the warmer box, imagine that a parcel of water is removed from the high latitude box, replaced by a cold, salt-free parcel having the same volume. Recalling $R > 1$, where $R = \beta S^*/\alpha T^*$ measures the relative effects of salinity and temperature on density, the reduced salt content will lead to lower density water in the cold box and hence a weaker circulation through the capillary.

The focus in this article has been placed on model development, with somewhat less attention given to the analysis of the system of ODEs (4.10). When teaching this material in the junior-level course MATH 305 *Mathematics and Climate*, I start with the pencil-and-paper approach presented in Chapter 6 in [5], teaching linearization at equilibria and the determination of the eigenvalue type via the trace and determinant of the Jacobian matrix along the way. Students then reinforce this analysis through their use of *Mathematica*.

Students are also exposed to introductory bifurcation theory in MATH 305, in which the Implicit Function Theorem plays an important role. Bifurcations of saddle-node,

Hopf, and cusp types are typically covered. In terms of Stommel's 2-box model, using *Mathematica* to see that one of the eigenvalues of the Jacobian matrix at the stable node (x_1^*, y_1^*) approaches 0 as the stable node and saddle point (x_2^*, y_2^*) merge in a saddle node bifurcation serves to reinforce the theory.

The bifurcation parameter λ is the proportionality constant for the flow rate through the capillary in Stommel's 2-box model. The flow resistance increases with λ, eventually leading to a single stable spiral equilibrium with an associated deep water flow from the low latitude box to the high latitude box. In this scenario the density difference is dominated by salinity. Insight into this behavior can be gleaned from the 1-basin model, where it was seen that salinity is the determining factor if the flow rate is sufficiently small (that is, λ is sufficiently large in the 2-box model setting).

While not presented here, it would be of interest to investigate how the model behaves as λ decreases toward 0, so that the flow resistance *decreases*. Does temperature then play the dominant role in determining density contrasts, as it does for increased flow rates in the 1-basin model?

Stommel's model provides for a wonderful introduction to the fundamental concepts of ocean circulation patterns. The corresponding ODEs are best analyzed via a combination of junior-level ODE analysis and the use of technology. This topic would make for an engaging addition to an upper-level mathematical modeling course.

Acknowledgment. Lecture notes on Stommel's model from a course offered by Professor Richard McGehee at the University of Minnesota served to frame the discussion of the model in MATH 305 as well as the presentation in this article. Professor McGehee's entire course on a mathematical approach to conceptual climate modeling—slides and lecture videos—can be found online [6].

Appendix

One can analyze Stommel's two-vessel model with the following *Mathematica* file. (We make no claims as to the efficiency of the code!)

```
(* Set λ here. We use δ = 1/6, R = 2 throughout. *)
Clear[λ]
λ = 0.2;

(* Here one can find the equilibrium flow rates fᵢ by solving equation (5.2)
  in the article for f. The value λ_0 =
 0.333801 is the saddle-node bifurcation value indicated in Figure 10 in the
   article.  *)
Clear[fequilibria, f1, f2, f3]
fequilibria = NSolve[λ * f == -1 / (1 + Abs[f]) + (2 / 6) / ((1 / 6) + Abs[f]), f];
If[ λ < 0.333801, {f1, f2, f3} = {fequilibria[[1]], fequilibria[[2]],
   fequilibria[[3]]}, f3 = fequilibria[[1]] ]
{{f → -1.06791}, {f → -0.307027}, {f → 0.21909}}

(* Here one finds the equilibria ((x*)ᵢ,(y*)ᵢ)
 corresponding to fᵢ via equation (5.1) in the article. *)
Clear[x1, y1, x2, y2, x3, y3]
If[ λ < 0.333801,
 {{x1, y1}, {x2, y2}, {x3, y3}} = {{(1 / 6) / ((1 / 6) + Abs[f]), 1 / (1 + Abs[f])} /. f1,
   {(1 / 6) / ((1 / 6) + Abs[f]), 1 / (1 + Abs[f])} /. f2,
   {(1 / 6) / ((1 / 6) + Abs[f]), 1 / (1 + Abs[f])} /. f3},
 {x3, y3} = {(1 / 6) / ((1 / 6) + Abs[f]), 1 / (1 + Abs[f])} /. f3]
{{0.134999, 0.48358}, {0.351845, 0.765095}, {0.432051, 0.820284}}

(* Here is the vector field given in equation (4.10) in the article *)
g[x_, y_, δ_] := δ * (1 - x) - Abs[(1 / λ) * (-y + 2 * x)] * x
h[x_, y_] := 1 - y - Abs[(1 / λ) * (-y + 2 * x)] * y

(* We split the vector field into the cases f =
 (1/λ)*(-y+2*x) < 0 and f = (1/λ)*(-y+2*x) ≥ 0 *)
gneg[x_, y_, δ_] := δ * (1 - x) - (- (1 / λ) * (-y + 2 * x)) * x
hneg[x_, y_] := 1 - y - (- (1 / λ) * (-y + 2 * x)) * y

gplus[x_, y_, δ_] := δ * (1 - x) - ((1 / λ) * (-y + 2 * x)) * x
hplus[x_, y_] := 1 - y - ((1 / λ) * (-y + 2 * x)) * y
```

```
(* Here's the Jacobian when f < 0 *)
MatrixForm[Jneg = {{D[gneg[x, y, 1 / 6], x], D[gneg[x, y, 1 / 6], y]},
   {D[hneg[x, y], x], D[hneg[x, y], y]}}]
```

$$\begin{pmatrix} -\frac{1}{6} + 10.\,x + 5.\,(2\,x - y) & -5.\,x \\ 10.\,y & -1 + 5.\,(2\,x - y) - 5.\,y \end{pmatrix}$$

```
(* Here's the Jacobian at (x1,y1) when f < 0 *)
If[λ < 0.333801, MatrixForm[J1 = Jneg /. {x → x1, y → y1}],
 Print["There are no equilibria with f < 0"]]
```

$$\begin{pmatrix} 0.115414 & -0.674995 \\ 4.8358 & -4.48581 \end{pmatrix}$$

```
(* Here are the evalues/evectors at (x1,y1) when f < 0 *)
If[λ < 0.333801, Eigenvalues[J1], Print["Only one equilibrium (x3,y3)"]]
If[λ < 0.333801, Eigenvectors[J1], Print["Only one equilibrium (x3,y3)"]]
```

```
{-3.60951, -0.760883}
```

```
{{0.178306, 0.983975}, {0.610234, 0.792222}}
```

```
(* Here's the Jacobian at (x2,y2) when f < 0 *)
If[λ < 0.333801, MatrixForm[J2 = Jneg /. {x → x2, y → y2}],
 Print["There are no equilibria with f < 0"]]
```

$$\begin{pmatrix} 3.04476 & -1.75922 \\ 7.65095 & -5.1325 \end{pmatrix}$$

```
(* Here are the evalues/evectors at (x2,y2) when f < 0 *)
If[λ < 0.333801, Eigenvalues[J2], Print["Only one equilibrium (x3,y3)"]]
If[λ < 0.333801, Eigenvectors[J2], Print["Only one equilibrium (x3,y3)"]]
```

```
{-2.84863, 0.760883}
```

```
{{0.286036, 0.958219}, {0.610234, 0.792222}}
```

```
(* Here's the Jacobian when f ≥ 0 *)
MatrixForm[Jplus = {{D[gplus[x, y, 1 / 6], x], D[gplus[x, y, 1 / 6], y]},
   {D[hplus[x, y], x], D[hplus[x, y], y]}}]
```

$$\begin{pmatrix} -\frac{1}{6} - 10.\,x - 5.\,(2\,x - y) & 5.\,x \\ -10.\,y & -1 - 5.\,(2\,x - y) + 5.\,y \end{pmatrix}$$

```
(* Here's the Jacobian at (x3,y3) when f > 0 *)
MatrixForm[J3 = Jplus /. {x → x3, y → y3}]
```

$$\begin{pmatrix} -4.70627 & 2.16025 \\ -8.20284 & 2.88233 \end{pmatrix}$$

```
(* Here are the evalues/evectors at (x3,y3) when f > 0 *)
Eigenvalues[J3]
Eigenvectors[J3]

(* Here is a plot of the equation f = 0 (green line),
the equilibria and the flowlines. Above the green line f <
 0 (temperature dominates density contrast),
while below the green line f > 0 (salinity dominates density contrast).
     The direction of the flow through the capillary stops and reverses
    along any trajectory crossing the green line. The value λ =
 0.333801 is the saddle-node bifurcation value indicated in Figure 10 in
    the above article. *)
If[λ ≤ 0.333801, Show[ContourPlot[(1 / λ) * (-y + 2 * x) == 0,
    {x, 0, 1}, {y, 0, 1}, ContourStyle → Directive[Darker[Green], Thick],
    FrameLabel → {"x (salinity)", "y (temperature)"}, LabelStyle → Bold],
  Graphics[{Red, Disk[{x, y} /. {x → x1, y → y1}, 0.01],
     Disk[{x, y} /. {x → x2, y → y2}, 0.01], Disk[{x, y} /. {x → x3, y → y3}, 0.01] }],
  StreamPlot[{g[x, y, 1 / 6], h[x, y]}, {x, 0, 1}, {y, 0, 1}]],
 Show[ContourPlot[(1 / λ) * (-y + 2 * x) == 0, {x, 0, 1}, {y, 0, 1},
    ContourStyle → Directive[Darker[Green], Thick],
    FrameLabel → {"x (salinity)", "y (temperature)"}, LabelStyle → Bold],
  Graphics[{Red, Disk[{x, y} /. {x → x3, y → y3}, 0.01] }],
  StreamPlot[{g[x, y, 1 / 6], h[x, y]}, {x, 0, 1}, {y, 0, 1}]]
]
```

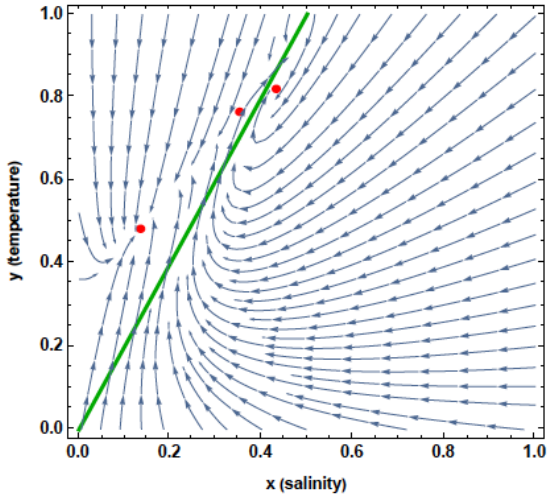

References

[1] R. Borrelli and C. Coleman. *Differential Equations: A Modeling Perspective*. Wiley, 2nd edition, 2004.

[2] M. Carlowicz. Watery heatwave cooks the Gulf of Maine. *NASA Global Climate Change Vital Signs of the Planet*, September 12, 2018. URL https://climate.nasa.gov/news/2798/watery-heatwave-cooks-the-gulf-of-maine/.

[3] T. DeVries, M. Holzer, and F. Primeau. Recent increase in oceanic carbon uptake driven by weaker upper-ocean overturning. *Nature*, 542:215–218, 2017.

[4] L.G. Henry, J.F. McManus, W.B. Curry, N.L. Roberts, A.M. Piotrowski, and L.D. Keigwin. North Atlantic ocean circulation and abrupt climate change during the last glaciation. *Science*, 353:10.1126/science.aaf5529, June 2016.

[5] H. Kaper and H. Engler. *Mathematics and Climate*. SIAM, 2013.

[6] R. McGehee. Math 5490 Fall 2014. URL http://www-users.math.umn.edu/~mcgehee/teaching/Math5490-2014-2Fall/lectures.html.

[7] M. Rhein, S.R. Rintoul, S. Aoki, E. Campos, D. Chambers, R.A. Feely, S. Gulev, G.C. Johnson, S.A. Josey, A. Kostianoy, C. Mauritzen, D. Roemmich, L.D. Talley, and F. Wang. *Observations: Ocean. In: Climate Change 2013: The Physical Science Basis. Contribution of Working Group I to the Fifth Assessment Report of the Intergovernmental Panel on Climate Change [Stocker, T.F., D. Qin, G.-K. Plattner, M. Tignor, S.K. Allen, J. Boschung, A. Nauels, Y. Xia, V. Bex and P.M. Midgley (eds.).* Cambridge University Press, 2013.

[8] T.F. Stocker, D. Qin, G.-K. Plattner, M. Tignor, S.K. Allen, J. Boschung, A. Nauels, Y. Xia, V. Bex, and P.M. Midgley (eds.). *IPCC, 2013: Summary for Policymakers. In: Climate Change 2013: The Physical Science Basis. Contribution of Working Group I to the Fifth Assessment Report of the Intergovernmental Panel on Climate Change*. Cambridge University Press, 2013.

[9] H. Stommel. Thermohaline convection with two stable regimes of flow. *Tellus*, 13(2): 224–230, 1961.

[10] D. Thornalley, D. Oppo, P. Ortega, J. Robson, C. Brierley, R. Davis, I. Hall, P. Moffa-Sanchez, N. Rose, P. Spooner, I. Yashayaev, and L. Keigwin. Anomalously weak Labrador Sea convection and Atlantic overturning during the past 150 years. *Nature*, 556:227–230, 2018.